Kinetics of deuteration of the $Pd_{0.772}Ag_{0.228}$ alloy with α/β phase transition by *in-situ* neutron diffraction

Michele Catti [a, *], Oscar Fabelo [b], Alessandra Filabozzi [c], Antonino Pietropaolo [d], Alessia Santucci [d], Silvano Tosti [d]

[a] *Dipartimento di Scienza dei Materiali, Università di Milano Bicocca, via Cozzi 55, 20125 Milano, Italy*
[b] *Institut Laue-Langevin, 71 avenue des Martyrs, 38000 Grenoble, France*
[c] *Dipartimento di Fisica, Università di Roma Tor Vergata, via della Ricerca Scientifica 1, 00133 Roma, Italy*
[d] *ENEA, Dipartimento Fusione e Tecnologie per la Sicurezza Nucleare, via Fermi 45, 00044 Frascati, Italy*

ABSTRACT

The deuteration reaction of a $Pd_{0.772}Ag_{0.228}$ foil was studied by neutron powder diffraction measurements vs. time in different T and $p(D_2)$ conditions (D20 and D2B high-resolution diffractometers at ILL, France). The system has great importance as permeable membrane for hydrogen separation. At $p = 1$ bar and $T < 200\,°C$ Bragg peak splitting indicates the presence of two cubic phases, to be identified with the α and β modifications of palladium hydride. Rietveld refinements provided the corresponding $a_α$ and $a_β$ lattice constants, the $\nu_α$ and $\nu_β$ occupancies of D, and the β phase volume fraction vs. time during deuteration progress. A continuous α → β transformation takes place till reaction end. At $T = 200\,°C$ or $p > 1$ bar a single phase was always observed. The phase diagram of $Pd_{0.772}Ag_{0.228}D_\nu$ is thus shown to present a α+β two-phase domain less extended but similar to that of PdH_ν, at variance with most thermodynamic measurements suggesting full single-phase behavior. The $\nu(t)$ kinetic data of deuteration at $80\,°C/1$ bar can be interpreted by a mechanism based on a first-order nucleation step followed by a zero-order step of surface adsorption and dissociation of the D_2 molecule.

© 2019 Elsevier B.V. All rights reserved.

1. Introduction

Palladium is well known to absorb large quantities of hydrogen into the octahedral cavity of the face-centred-cubic metal framework, producing the non-stoichiometric PdH_ν hydride; therein the H-to-metal ratio ν can attain about 0.7 at room temperature and pressure [1,2]. A characteristic feature is that two FCC modifications with slightly different lattice constants may coexist in the solid hydride below $290\,°C$: the H-poor α and the H-rich β phases [3].

The H absorbing properties of Pd are of extreme importance for the technology of hydrogen as energy carrier from renewable sources [4,5]. This concerns particularly the steps of production, storage and separation, which rely on applications of catalysis properties and on use of permeable membranes [6,7]. Such devices should be designed to achieve very high hydrogen permeability and selectivity, and then to provide the best solution for separating H_2 from other gases and/or to purify it. However, an unfavorable issue

of Pd membranes is that embrittlement often occurs after repeated H absorption/desorption cycling, with deterioration of the mechanical properties [7]. This effect has been ascribed to the strain induced by a 10% volume change in the α/β phase transition [8—10]. Attempts to solve the problem by alloying Pd with other metals have led to select the $Pd_{0.772}Ag_{0.228}$ composition as best material for H permeable membranes. Such alloy is reported to form the $Pd_{0.772}Ag_{0.228}H_\nu$ hydride with $\nu \leq 0.4$ in ambient conditions [11] and with reduced embrittlement problems, so as to be employed successfully as hydrogen permeable membrane in industrial processes [6,7]. Indeed, Pd alloys with silver content over 20%—30% are claimed to present a single hydride phase at room temperature [12], but some peculiar aspects of electrical resistivity at higher T would hint at a possible phase transition [13]. So the problem of an accurate phase diagram for the $Pd_{0.772}Ag_{0.228}H_\nu$ limit composition is still open.

We have thus undertaken a research on the $Pd_{0.772}Ag_{0.228}D_\nu$ system at different temperatures and pressures by *in-situ* neutron powder diffraction, in order to investigate the structural aspects of the deuterium absorption/desorption reactions in the palladium-

silver alloy. In the first experiment, performed by a medium-resolution equipment, the D/M ratio ν was determined as refined D occupancy in the FCC octahedral site in various T and p conditions [14]. Further experiments were then carried out on high-resolution/high-flux diffractometers, with the purpose of resolving the possible presence of two phases and following the reaction progress with time. The results of such measurements are presented here, discussing implications for the phase diagram of $Pd_{0.772}Ag_{0.228}D_\nu$ and for the kinetics of the deuteration process.

2. Experimental

2.1. Neutron diffraction measurements

The same thin foil specimen of $Pd_{0.772}Ag_{0.228}$ alloy (Goodfellow Cambridge Ltd.) used in the previous experiment [14], with the corresponding thermal/absorption-desorption history, was rolled up in an aluminum can and employed in the present study. Diffraction intensities were measured on the D2B and D20 neutron diffractometers at ILL (Grenoble, France), providing a better resolution ($\Delta d/d \approx 5 \times 10^{-4}$ and 10^{-3}, respectively) than that of D1B used previously (5×10^{-3} to 10^{-2} range). Most data were collected on high-intensity D20, which allows very short collection times for a full diffraction pattern and is thus most suitable for kinetic studies ($2\theta = 1–153°$, $\lambda = 1.5420$ Å from Ge(115) monochromator; measurement time = 5–15 min). In the D2B case ($\lambda = 1.5942$ Å from Ge(335) monochromator, $2\theta = 1–160°$) a total 2.7 h time was employed for a full data collection, which is however obtained by merging the neutron counts from 10 angular scans of the multi-detector (1.25° and 16 min each) collected consecutively and stored separately. The sample holder was connected to a gas manifold equipped with vacuum turbomolecular pump (10^{-6} bar), a D_2 cylinder, a mass flow controller and a pressure sensor, so as to set and control the pressure of deuterium inside; temperature was measured by two suitably positioned thermocouples.

A diffraction pattern was collected on the empty aluminum can inside the pressure cell, and it was analysed by profile matching. The result was included as an additional phase in all subsequent refinements of deuterated $Pd_{77}Ag_{23}$ to cope with the Al peaks.

In the D20 experiment, kinetic measurements of the absorption of D_2 into the $Pd_{0.772}Ag_{0.228}$ alloy were performed in isothermal conditions at 80, 150 and 200 °C. On heating the sample in vacuum the appropriate temperature was attained, and after a 30 min stabilization time deuterium gas was let in and three subsequent kinetic cycles at $p(D_2) = 1$, 4 and 8 bar were carried out. Then the sample was heated in vacuum to the next T value, repeating the three cycles at different pressures. Each cycle was made up of consecutive collections of diffraction patterns (measurement time: 10 min for 80 °C/1 bar and 80 °C/4 bar; 5 min in all other cases), till no changes appeared in the diffractograms so that the absorption process could be considered to be completed. At the cycle end a final pattern was measured for 15 min. The three temperatures were attained consecutively on heating, unlike the previous experiment [14] where the sample was heated each time to 200 °C before cooling to the wanted temperature. The present procedure was chosen to save time for the long kinetic measurements, because cooling is very time-consuming. On the other hand, in the D2B experiment the sample was heated in vacuum to 200 °C, it was filled with D_2 at 1 bar, and then it was cooled to 80 °C at constant pressure, collecting diffraction patterns during deuteration due to cooling. Then the alloy was evacuated and heated again to 200 °C, it was filled with D_2 at 4 bar, it was evacuated, filled with D_2 at 1 bar, and cooled to 80 °C at constant pressure, again collecting diffraction patterns on deuteration subsequent to cooling.

2.2. Crystal structure analysis

The diffraction profile of each pattern was refined by the multi-phase technique implemented in the Fullprof computing package [15]. The FCC deuterated alloy $Pd_{0.772}Ag_{0.228}D_\nu$ was Rietveld-refined with four structural parameters: unit-cell edge a, displacement factors B of the average $Pd_{0.772}Ag_{0.228}$ atom (located at 0, 0, 0) and of the D atom (at ½, 0, 0), and D occupation factor (o.f.). Aluminum from the sample holder was treated as additional phase by profile matching with constant relative intensities; only the unit-cell constant and the scale factor were refined, keeping fixed the other profile parameters from the calibration results of the empty cell. The background intensity was linearly interpolated by a set of fixed points. Bragg peaks were modelled by a linear combination of Gaussian and Lorentzian components (pseudo-Voigt function), with σ and γ half-widths, respectively. The σ and γ parameters varied with the diffraction angle θ as $\sigma = (U \tan^2\theta + V \tan\theta + W)^{1/2}$ and $\gamma = Y/\cos\theta$. The mixing coefficient and the full width of the pseudo-Voigt function depend on σ and γ according to equations given in the literature [16]. The scale factor and the U, V, W, Y profile parameters of the $Pd_{0.772}Ag_{0.228}D_\nu$ phase were always refined. Neutron scattering lengths are 6.671 (D), 5.910 (Pd), and 5.922 (Ag) fm; cf. the very similar Pd and Ag values, which make the metal contribution to diffraction intensity hardly sensitive to compositional variations of the alloy.

3. Results and discussion

3.1. Equilibrium structure

At first, equilibrium results at a given temperature and $p(D_2)$ pressure, obtained when the process of deuterium absorption was completed, are presented. In Tables 1 and 2 the refined structural parameters and the R_p (profile), wR_p (weighted profile), and R_B (Bragg peak intensity) agreement indexes are reported for the sets of D2B and D20 measurements, respectively.

By using the technique of Fourier difference maps, and exploiting the high resolution and very good quality of the collected diffraction data, we checked the issue of possible fractional location of the D atom off the ½, 0, 0 octahedral site. With both D2B and D20 data some weak difference peaks appeared in the maps, and one of them could be included successfully in the refinement. In the case of the D2B pattern at 80 °C the 0.25 0.25 0.11(1) position was refined for the second D atom, corresponding to two D-(Pd,Ag) distances of 1.49(1) Å and two of 2.10(3) Å ($R_p = 6.8\%$, $wR_p = 10.3\%$, $R_B = 2.2\%$). This location is somewhat displaced from the ¼, ¼, ¼ tetrahedral site considered by previous work as secondary D position in PdH_ν [17,18]. However, an occupancy factor of only 0.008(1) was obtained, corresponding to about 2% of the refined D occupancy on the ½, 0, 0 site, and within its experimental error (cf. the e.s.d. = 0.015 in Table 1). Thus we considered the possible extra-octahedral contribution to deuterium absorption to be negligible in all subsequent refinements.

The deuterium occupancies from D2B measurements (Table 1) are quite similar to the values considered to be at equilibrium (at the same temperatures) in our previous study [14]. However, the corresponding D20 results (Table 2) appear to be slightly lower. This may be related to the different thermal cycle adopted in the latter case for practical reasons specific of the extensive D20 kinetic measurements. Nevertheless the results reported below should not be affected by this small effect, as is shown by consistency of D2B and D20 kinetic data (cf. the next section).

3.2. Kinetic study: α/β two-phase evidence

Most diffraction patterns recorded during isothermal deuterium

Table 1
Results of Rietveld refinements of $Pd_{0.772}Ag_{0.228}D_\nu$ after completion of deuterium absorption at two temperature values (D2B measurements). E.s.d.'s in parentheses.

T (°C)	$p(D_2)$ (bar)	R_p (%)	wR_p (%)	R_B (%)	a (Å)	o.f.(D) = ν	B(Pd/Ag) (Å²)	B(D) (Å²)
80	1	6.9	10.4	4.6	4.01476(3)	0.384(15)	0.52(5)	4.8(3)
200	1	7.0	10.2	3.4	3.96740(3)	0.131(12)	0.526(2)	2.9(6)

Table 2
Results of Rietveld refinements of $Pd_{0.772}Ag_{0.228}D_\nu$ at the end of kinetic cycles of deuterium absorption at different temperatures and pressures (D20 measurements). E.s.d.'s in parentheses.

T (°C)	$p(D_2)$ (bar)	R_p (%)	wR_p (%)	R_B (%)	a (Å)	o.f.(D) = ν	B(Pd/Ag) (Å²)	B(D) (Å²)
80	10^{-6}	8.4	12.6	6.3	3.93153(3)	0	0.88(2)	–
80	1	6.3	9.3	2.8	4.01650(3)	0.326(7)	1.08(3)	4.4(1)
80	4	6.1	9.2	2.0	4.02171(3)	0.363(8)	1.28(3)	5.4(2)
80	8	5.5	8.4	2.1	4.02465(3)	0.371(7)	1.32(3)	5.2(1)
150	1	6.4	10.0	3.1	3.99836(3)	0.199(7)	1.06(3)	3.5(2)
150	4	6.0	9.4	3.2	4.01527(3)	0.240(8)	0.92(3)	3.5(2)
150	8	5.8	9.2	2.7	4.02030(3)	0.262(7)	0.98(3)	3.8(2)
200	1	6.7	11.1	2.8	3.96753(3)	0.079(5)	1.30(3)	1.2(4)
200	4	6.1	9.8	3.4	4.00381(3)	0.190(7)	1.13(3)	3.5(2)
200	8	5.6	9.1	2.6	4.01342(3)	0.221(7)	1.08(3)	3.9(2)

absorption showed a very peculiar aspect. In Fig. 1 the diffracto-gram measured at 80 °C after 70 min of 1 bar D_2 uploading (out of 340 min necessary to finish the process) is displayed. All FCC Bragg peaks appear to be split, and with increasing time the intensity ratio of each pair varies continuously in favor of the peak at lower 2θ. This was quite unexpected, because no such splitting was observed in the previous similar experiment at lower resolution [14]. It is thus concluded that two distinct FCC phases of $Pd_{0.772}Ag_{0.228}D_\nu$ form in the sample during the process; one of them grows at the expense of the other one, till the sample becomes single phase once the D_2 absorption is completed.

Such phases are clearly to be identified with the α and β modifications of palladium hydride [19–21]. However, one of them is

here observed in metastable rather than equilibrium conditions, as it transforms into the other phase on passing time. A magnified portion of the set of all diffraction patterns collected in the course of the kinetic experiment at $T = 80$ °C, $p(D_2) = 1$ bar is shown in Fig. 2. The trend of peak intensity vs. time allows us to understand how the two-phase sample of $Pd_{0.772}Ag_{0.228}D_\nu$ transforms during progressive deuteration: the α modification, with smaller unit-cell and less D content, changes continuously into the D-richer β phase with larger cell.

The same result is shown by the D2B measurements, which however concern deuterium absorption obtained by cooling (from 200 to 80 °C) rather than by pressure increase (from vacuum to 1 bar) as in the D20 case. In Fig. 3 the diffraction intensity is displayed as coloured contour areas vs. 2θ angle and number of the
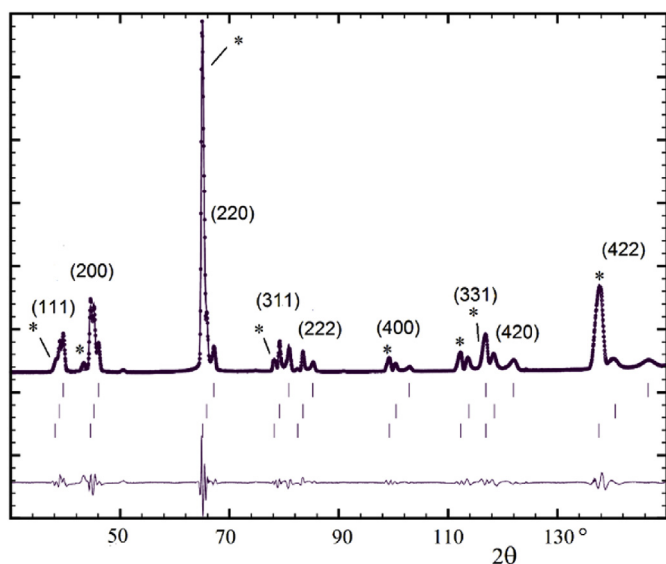

Fig. 1. Neutron powder diffraction pattern of two-phase (α+β) $Pd_{0.772}Ag_{0.228}D_\nu$ during deuterium absorption at $T = 80$ °C, $p(D_2) = 1$ bar (D20 diffractometer, $\lambda = 1.5420$ Å). Small vertical bars denote the Bragg peak positions for the α and β phases (upper and middle rows), and for Al of the pressure cell (lowest row, also emphasized by asterisks). The difference (observed minus calculated) profile from Rietveld refinement is shown below. Indexes *hkl* of Bragg peaks are given.
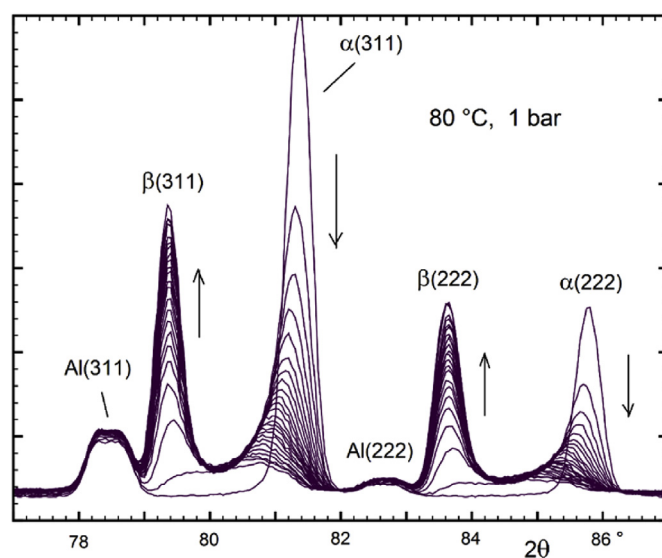

Fig. 2. Isothermal α (D-poor) to β (D-rich) phase transformation of $Pd_{0.772}Ag_{0.228}D_\nu$, as the ν uptake of deuterium increases after raising $p(D_2)$ from 10^{-6} to 1 bar at $T = 80$ °C. Arrows indicate the direction of increasing time. The 77–87° angular range, including the (311) and (222) Bragg peaks from each phase, is shown out of 30 diffraction patterns (D20 diffractometer, $\lambda = 1.5420$ Å) of 10 min duration each.
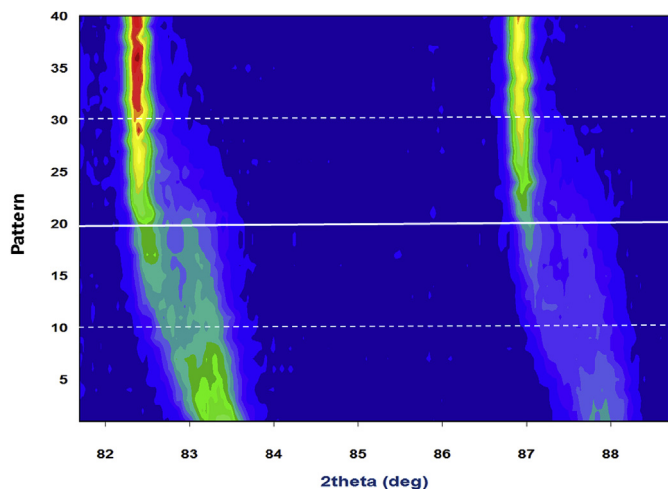
Fig. 3. Isobaric α (D-poor) to β (D-rich) phase transformation of $Pd_{0.772}Ag_{0.228}D_\nu$, as the ν uptake of deuterium increases after lowering *T* from 200 to 80 °C at $p(D_2) = 1$ bar. The angular range including the (311) and (222) Bragg peaks from each phase is shown out of 4×10 diffraction patterns (D2B diffractometer, $\lambda = 1.5942$ Å) of 16 min duration each. Time increases with the pattern number.

pattern. Four different measurements, each including a set of 10 patterns (cf. the Experimental section), are included in the graph. In the D20 kinetic measurements at 150 °C, 1 bar a similar α → β transformation is observed as at 80 °C, but with a smaller 2θ splitting of Bragg peaks (Fig. 4). This means that on increasing temperature the volume difference between the two coexisting phases decreases progressively, and indeed at 200 °C/1 bar the sample remains single-phase throughout the whole deuteration reaction. Also all kinetic results obtained with $p = 2$ and 4 bar at any temperature show a single-phase behavior of the system.

Rietveld refinements of all recorded patterns were carried out in the three-phase or two-phase mode (including Al from pressure cell) appropriately. In the former case the lattice constants a_α and a_β, and the deuterium occupancies ν_α and ν_β were refined for each cubic phase of $Pd_{0.772}Ag_{0.228}D_\nu$; the volume ratio of the two phases was refined as well, yielding the β volume fraction $\xi = V_\beta/(V_\alpha+V_\beta)$. Thus, the total D content per formula-unit could be obtained as
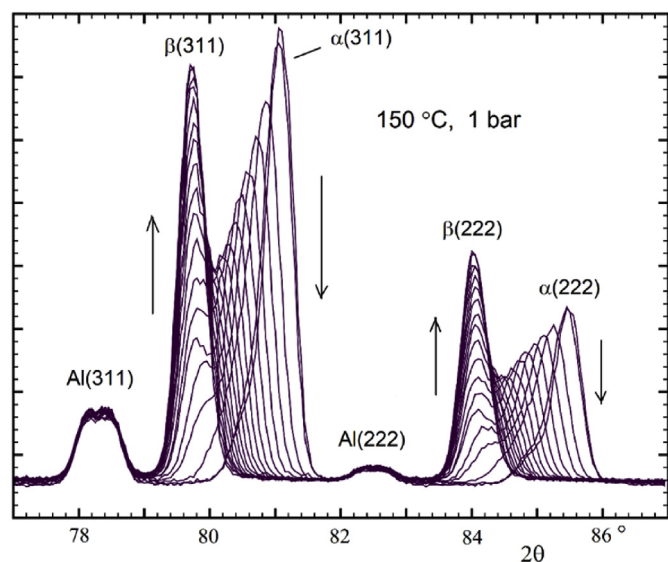
weighted average of the two occupancies $<\nu> = (1-\xi)\nu_\alpha+\xi\nu_\beta$. In Fig. 5 the refined unit-cell constants are plotted against time for all experiments; their e.s.d.'s are not larger than 10^{-4} Å for the β or single-phase values, while the α values range between 10^{-4} and 4×10^{-4} Å. At $p(D_2) = 1$ bar, the gap between a_α and a_β appears clearly to shrink with deuteration progress, and it is much smaller at 150 than at 80 °C. Results obtained at higher pressure (black symbols) always correspond to a single phase.

For the deuteration reaction at 80 °C and 1 bar, the β phase fraction ξ is plotted vs. time in Fig. 6, and the corresponding plots of the ν_α, ν_β and $<\nu>$ occupancies are displayed in Fig. 7. The deuterium content of the two phases appears to change little during the reaction progress, so that the curve of the average occupancy $<\nu>$ resembles closely that of the β phase fraction ξ. During deuteration it is interesting to remark that, while both a_β and ν_β remain constant, the volume of the α phase increases significantly despite the little variation of ν_α (cf. Figs. 5 and 7). This would suggest that the denser α lattice is not able to absorb deuterium without expanding, at variance with the β phase whose larger volume does not need further expansion on absorption. Results obtained at 150 °C/1 bar (Fig. 8) are less accurate, because the ν_α and ν_β occupancies are quite close to each other so that the e.s.d.'s of their refined values increase significantly. Therefore, also the average value $<\nu>$ (plotted in Fig. 8 for the first part of the reaction) is affected by a large uncertainty, whereas after 60 min a single phase model had to be adopted with an ensuing lower error of the ν occupancy. The trend of single-phase D content ν vs. absorption time at higher pressure (2 and 4 bar) is shown as well (closed symbols) in Fig. 8.

The kinetic behavior of the α and β phase volumes and D occupancies at different *T, p* conditions, such as displayed in Figs. 5−8, can be represented by aid of a qualitative phase diagram of the solid $Pd_{0.772}Ag_{0.228}D_\nu$ system. This is sketched in Fig. 9 as a sequence of $p(\nu)$ isotherms, which show the miscibility gap of atomic deuterium D into the $Pd_{0.772}Ag_{0.228}$ alloy. A two-phase α+β domain arises below a critical temperature lying between 150 and 200 °C. All kinetic experiments of isothermal deuterium absorption performed on D20, triggered by pressure increase, are represented qualitatively as P_iQ_i (*p* from 10^{-6} to 1 bar) and Q_iR_i (*p* from 1 to 4 and to 8 bar) segments of isotherms. Also the D2B isobaric experiment,
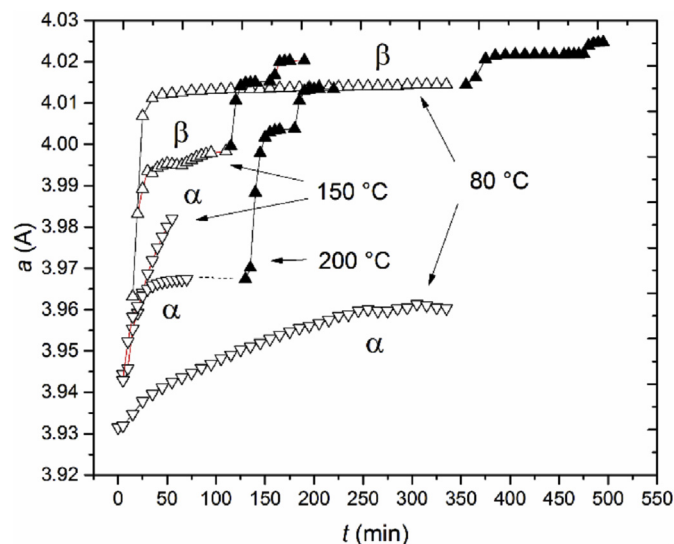

Fig. 4. Results similar to those of Fig. 2 at 150 °C for 18 patters of 5 min duration each.

Fig. 5. Time evolution of the cubic unit-cell edge of the phases of $Pd_{0.772}Ag_{0.228}D_\nu$ during deuterium absorption at $p(D_2) = 1$ bar (open symbols) and 4 and 8 bar (closed symbols), at three different temperatures. Data at 200 °C and p > 1 bar are shifted by 50 min on the time scale to avoid superposition.
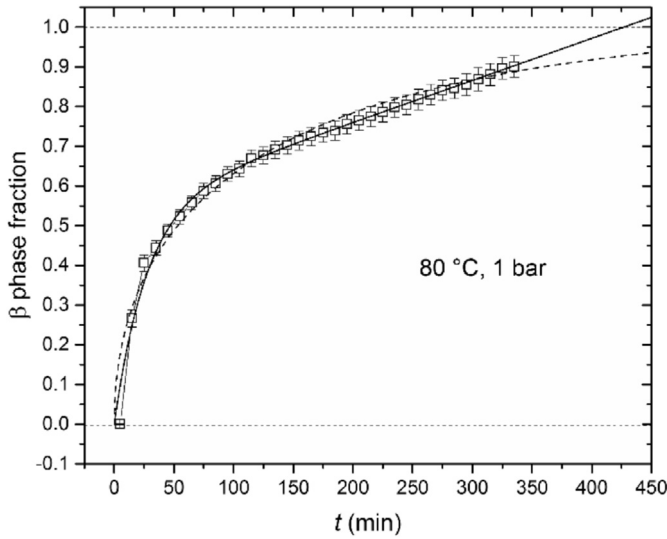
Fig. 6. Volume β phase fraction $\xi = V_\beta/(V_\alpha + V_\beta)$ from Rietveld refinements of $Pd_{0.772}Ag_{0.228}D_\nu$ during the progressive isothermal D_2 absorption. The solid and dashed curves correspond to the fitting function given in Table 3 and to $\xi = 1 - [1 - (0.0008t)^{1/2}]^3$, respectively.
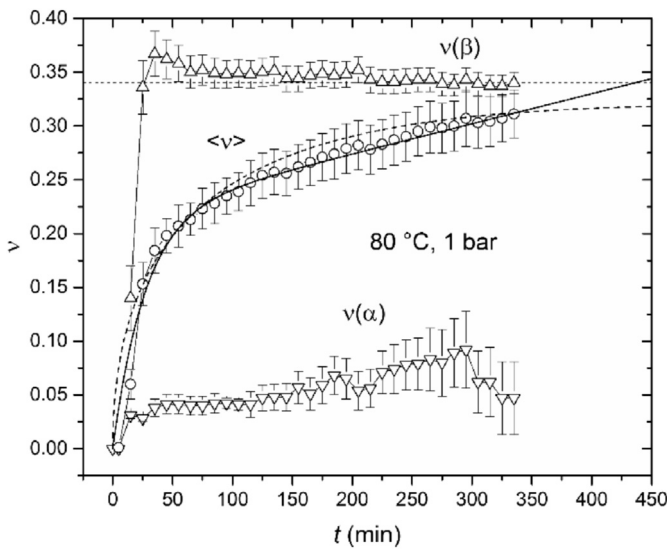

Fig. 7. Occupancy ν of deuterium D in each of the α and β phases of $Pd_{0.772}Ag_{0.228}D_\nu$, and weighted average $<\nu> = (1 - \xi)\nu_\alpha + \xi\nu_\beta$, against D_2 absorption time. The solid and dashed curves correspond to the fitting function given in Table 3 and to $<\nu> = 0.34\{1 - [1 - (0.0015t)^{1/2}]^3\}$, respectively.

Fig. 8. Two-phase average $<\nu>$ (150 °C, $t < 60$ min) and single-phase ν (all other cases) occupancies of deuterium in $Pd_{0.772}Ag_{0.228}D_\nu$ against D_2 absorption time, at 1 bar (open circles) and at 4 (closed circles) and 8 bar (closed squares). Thick curves for 1 and 4 bar kinetics correspond to Avrami fitting functions reported in Table 3.
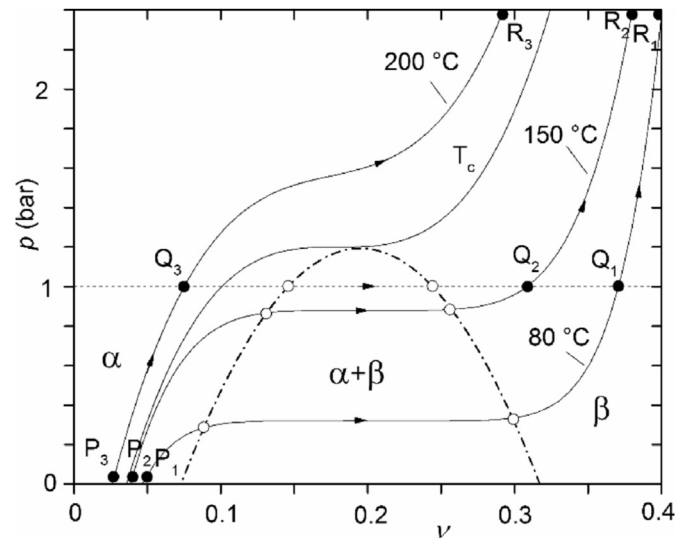
Fig. 9. Sketch of a qualitative phase diagram of $Pd_{0.772}Ag_{0.228}D_\nu$, suggested by kinetic measurements of the deuterium uptake process. The $\alpha + \beta$ two-phase region is bounded by a dotted-dashed line. P_1Q_1, P_2Q_2 and P_3Q_3 correspond to the isothermal experiments performed at 80 (Fig. 2), 150 (Fig. 4) and 200 °C on D20, after raising $p(D_2)$ from 10^{-6} to 1 bar; similarly, Q_1R_1, Q_2R_2 and Q_3R_3 after raising pressure from 1 to 4 and to 8 bar (out of scale). Q_3Q_2 denotes the isobaric experiment performed at 1 bar on D2B (Fig. 3), after decreasing T from 200 to 80 °C.

where absorption was induced by a 200 to 80 °C temperature decrease, is included as constant pressure segment Q_3Q_2. Thus, the two-phase $\alpha + \beta$ assemblage was observed in our experiments in metastable conditions only, during the processes of adjustment of the lower pressure of the system to the higher external pressure, or of the higher system temperature to the lower external one, which led eventually to stable single-phase systems. For instance, from the experiment at 80 °C with p raised from 10^{-6} to 1 bar, we can surmise that at that temperature the $\alpha + \beta$ assemblage would be stable at a pressure surely lower than 1 bar (cf. the plateau of the isotherm in Fig. 9). Of particular interest is the outcome of isobaric cooling from 200 to 80 °C at 1 bar: the corresponding equilibrium isotherm with two-phase plateau is guessed to occur slightly above 150 °C (Fig. 9). This means that the phase transformation of
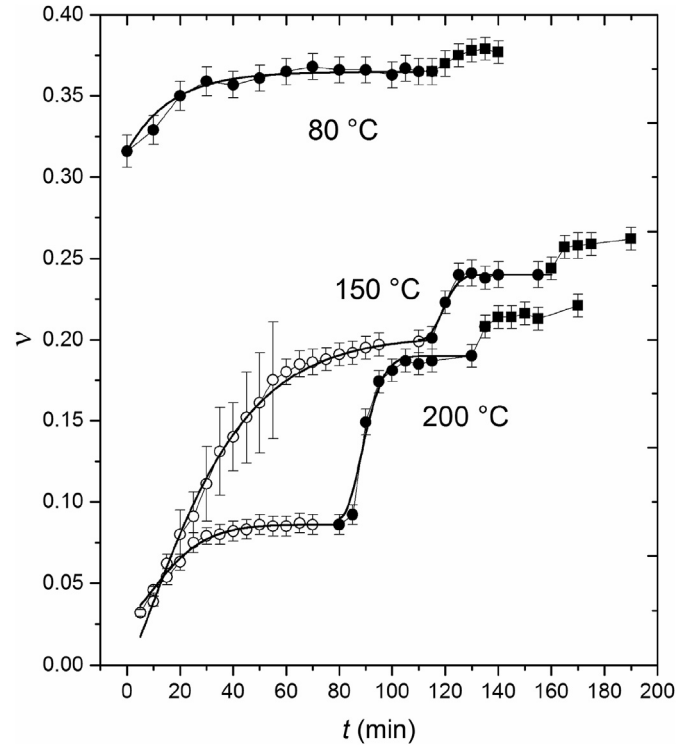
$Pd_{0.772}Ag_{0.228}D_\nu$ would take place around 160 °C at room pressure, thus accounting in terms of an α/β phase transition for the minimum of electrical resistivity observed at about 140 °C in the hydride of $Pd_{0.79}Ag_{0.21}$ [13].

Results obtained for lattice constants and deuterium content of the α and β phases of $Pd_{0.772}Ag_{0.228}D_v$ at 80 °C/1 bar, can be compared to the known behavior of the corresponding phases of PdD_v in the same conditions. In the latter case $v_\alpha = 0.02$ and $v_\beta = 0.57$ are observed [2], to be compared to 0.05 and 0.35 (Fig. 7) for the deuterated Pd-Ag alloy. Thus, the D solubility in the α phase increases slightly but significantly when Ag is alloyed with Pd. This may be interesting in relation to recent results on the end member α-PdH_v, which suggest a covalent Pd-H bonding in α vs. a metallic one in the β phase [22]. Replacing Pd by Ag may indeed favor the covalent with respect to metallic bond, thus raising the D solubility in the α phase. On the other hand, the smaller D content of β-$Pd_{0.772}Ag_{0.228}D_v$ with respect to β-PdD_v seems to be simply related to the larger total H/D solubility in pure than in alloyed Pd. Another relevant difference is given by the critical temperature, which is about 290 °C for PdH_v [1–3] but it seems to lie at least 100 °C below in the case of $Pd_{0.772}Ag_{0.228}D_v$.

Direct thermodynamic measurements of the isotherms of the $Pd_{1-x}Ag_x$-H system are reported by several authors [23–25]. It is claimed that, on increasing x_{Ag}, the $\alpha+\beta$ two-phase region shrinks progressively and disappears for $x_{Ag} > 0.24$ at 303 K, and for $x_{Ag} > 0.15$ at 423 K [23]. Indeed, for the $x_{Ag} = 0.23$ limit value a true pressure plateau was hardly observed at any temperature in the reported isotherms. However, due to the known difficulties in achieving equilibrium results in PCI (pressure-composition-isotherm) measurements, it cannot be excluded that, in limit conditions, the miscibility gap may be missed by that experimental technique.

As a concluding remark, the thermal/absorption-desorption history and the physical features of samples on which experiments are performed may affect the phase behavior of $Pd_{0.772}Ag_{0.228}D_v$, unless a proper sample activation is carried out. In our work the same single specimen was used for all previous [14] and present measurements, with similar thermal activation cycles, so that the different results are comparable. It could be interesting to study the behavior of different samples in a more extensive investigation.

3.3. Kinetic study: deuteration reaction modelling

The degree of advancement α of the deuteration reaction can be generally represented by the ratio v/v_{max} (single-phase) or $\langle v \rangle/\langle v_{max} \rangle$ (two-phase condition), where v_{max} is the equilibrium D occupancy reached at reaction end. However, as there is some uncertainty in defining the end value v_{max} exactly, we shall prefer to consider the non-normalized $v(t)$ or $\langle v \rangle(t)$ quantities as kinetic functions. In the two-phase case, the role of degree of advancement is also played by the β volume fraction $\xi = V_\beta/(V_\alpha + V_\beta)$, as v_β remains stable when the α phase is consumed (Fig. 7). Therefore, on the basis of results plotted in Figs. 6–8 it was possible to fit the corresponding data to different kinetic models [26,27]. The widely used Avrami equation $\alpha = 1 - \exp[-(kt)^n]$ is based on a nucleation-growth model, where the empirical parameter k is the reaction rate constant and n is related to the dimensionality of growing particles. Another popular kinetic formula, $\alpha = 1 - [1 - (kt)^{1/2}]^3$, is derived from the contraction-volume/diffusion scheme.

By trying to fit reaction data at 80 °C/1 bar (Figs. 6 and 7) to such equations, the Avrami model failed completely to account for the quasi-linear behaviors of plots in the final stage of the process. A better agreement was obtained by the contraction-volume/diffusion formula (dashed curves in Figs. 6 and 7); however, also in this case there are problems with the final reaction stage, as on extrapolation one would obtain reaction end ($\xi = 1$ in Fig. 6) at $t = 1/k = 1250$ min, which seems really too long when compared to the actual experimental curve. It was thus necessary to split the

process into two steps, assuming a zero-order kinetics (constant rate) at $t > 110$ min which accounts explicitly for the observed linear behavior in the late reaction stage: $\xi = 0.001060(7) t + 0.5481(17)$ was obtained by linear regression of data. The first step ($t < 110$ min) could still be modelled by the previous contraction-volume formula with $k = 8 \times 10^{-4}$ min^{-1}, but a better overall fit was obtained by combining a simple first-order kinetic law for the first step with the zero-order formula for the second one into a single equation. The resulting formulas for $\xi(t)$ and $\langle v \rangle(t)$ are reported in Table 3; the corresponding fitting curves are shown as thick lines in Figs. 6 and 7, respectively.

The process governed by first-order kinetics, much faster than the subsequent one, can be simply interpreted by a mechanism of nucleation of β phase domains within the α matrix. The second, slower process is accounted for by adsorption and dissociation of molecular D_2 on the surface of the sample, in presence of an excess of deuterium gas at constant pressure justifying the constant reaction rate. A parallel, complementary zero-order kinetic process could be the one-dimensional growth of β nuclei perpendicularly to the alloy foil surface. The constant rate process becomes rate-determining step of the whole reaction only when formation of β nuclei has stopped (about 110 min after deuteration start). Diffusion of atomic deuterium inside the alloy, which must occur in any case, looks like a much faster process than either of the two proposed steps of the deuteration reaction, so as not to affect its kinetics. Indeed, diffusivity D of deuterium in Pd and Pd-Ag alloys is reported in the range $3-8 \times 10^{-11}$ m^2 s^{-1} (at 80 °C) [28–30]; thus, the $d = 0.05$ mm thick foil would be passed through in a time ($= d^2/D$) of the order of 1 min, which is much less than the observed process duration.

In all other T, p conditions different from 80 °C/1 bar the results of phase fraction refinements were numerically too noisy to allow the $\xi(t)$ fitting to discriminate among different kinetic models. This was instead possible for the D content $\langle v \rangle$ or v at 1 and 4 bar, whereas in deuteration reactions at 8 bar the data quality was insufficient for reliable fittings also of the v quantity (Fig. 8). In no case any linear regime was detected, such as that observed in the reaction at 80 °C, 1 bar. Instead, a single fitting of the Avrami type was always able to account for the experimental behavior very satisfactorily. This seems to indicate that, at $T > 80$ °C the rate of β nuclei growth, and at $p > 1$ bar the deuterium adsorption rate are enhanced so that the zero-order kinetic process is no more rate-determining step. The fitted parameters are reported in Table 3, and the corresponding curves are shown as thick lines in Fig. 8. The time zero for equations in Table 3 is the instant when pressure was raised to the current value; of course this is not $t = 0$ in Fig. 8 for reactions at 4 bar.

4. Conclusions

The deuteration reaction of the $Pd_{0.772}Ag_{0.228}$ alloy has been monitored vs. time by a direct microscopic probe, the neutron beam, in different thermodynamic conditions. Sequences of intermediate metastable states have been detected during progress towards equilibrium, thus providing evidence of the α/β miscibility gap in the phase diagram of $Pd_{0.772}Ag_{0.228}D_v$, similarly to PdD_v and PdH_v. This clarifies an open point in the study of hydrides of the $Pd_{1-x}Ag_x$ alloys, as the $x = 0.23$ composition, of great importance for use as hydrogen permeable membrane, was claimed to be at the lower limit of single-phase only hydrides. Further, the α/β phase transition at room pressure is estimated to occur slightly above 150 °C, consistent with the minimum of electrical resistivity reported at 140 °C for the hydride of $x = 0.21$ composition. In summary, a quite smaller $\alpha+\beta$ two-phase domain is observed for $Pd_{0.772}Ag_{0.228}D_v$ than for pure PdD_v, with a critical temperature estimated to be

Table 3
Fitting functions of the β phase fraction and of the D occupancy vs. time during kinetic runs at different temperatures and pressures.

T (°C)	$p(D_2)$ (bar)	β phase fraction	D occupancy
80	1	$\xi = 0.548[1-\exp(-0.037t)] + 0.00106t$	$\langle \nu \rangle = 0.218[1-\exp(-0.037t)] + 0.00028t$
80	4		$\nu = 0.049[1-\exp(-0.060t)] + 0.316$
150	1		$\langle \nu \rangle = 0.202\{1-\exp[-(0.029t)^{1.25}]\}$
150	4		$\nu = 0.040\{1-\exp[-(0.090t)^{2.5}]\}+0.200$
200	1		$\nu = 0.056\{1-\exp[-(0.050t)^{1.5}]\} + 0.03$
200	4		$\nu = 0.10\{1-\exp[-(0.085t)^{2}]\}+0.09$

lower by over 100 °C, but the miscibility gap is clearly present yet.

Progress with time of the deuteration reaction could be quantitatively determined and fitted to suitable kinetic models. It turns out that, while at higher temperature a classic Avrami model (nucleation + growth single step) is quite adequate to account for results, at $T = 80$ °C the mechanism of reaction includes two steps. The first one is nucleation of the hydride phase in the alloy bulk with first-order kinetics. The second step, corresponding to adsorption and dissociation of deuterium gas on the sample surface, follows a zero-order kinetics and becomes rate-determining after that nucleation has come to end.

References

[1] F.D. Manchester, A. San-Martin, J.M. Pitre, in: Phase Diagrams of Binary Hydrogen Alloys, American society of Metals, 2000, p. 158.

[2] D.J. Safarik, R.B. Schwarz, S.N. Paglieri, R.L. Quintana, D.G. Tuggle, D.D. Byler, Composition dependence of the elastic constants of β-phase and [α+β]-phase PdH$_x$, Ultrasonics 50 (2010) 155–160.

[3] T.B. Flanagan, W.A. Oates, The palladium-hydrogen system, Annu. Rev. Mater. Sci. 21 (1991) 269–304.

[4] M.F. Orhan, I. Dincer, M.A. Rosen, M. Kanoglu, Integrated hydrogen production options based on renewable and nuclear energy sources, Renew. Sustain. Energy Rev. 16 (2012) 6059–6082.

[5] O. Biccikovci, P. Straka, Production of hydrogen from renewable resources and its effectiveness, Int. J. Hydrogen Energy 37 (2012) 11563–11578.

[6] J. Shu, B.P.A. Grandjean, A. Van Neste, S. Kalaguine, Catalytic palladium-based membrane reactors: a review, Can. J. Chem. Eng. 69 (1991) 1036–1060.

[7] S. Tosti, Pd-based membranes and membrane reactors for hydrogen production, in: H. Hilal, A.F. Ismail, C.J. Wright (Eds.), Membrane Fabrication, Ch. 13, CRC Press, Taylor & Francis Group, 2015, ISBN 978-1-4822-1045-3.

[8] G.S. Burkhanov, N.B. Gorina, N.B. Kolchugina, N.R. Roshan, Palladium-based alloy membranes for separation of high purity hydrogen from hydrogen-containing gas mixtures, Platin. Met. Rev. 55 (2011) 3–12.

[9] F.A. Lewis, K. Kandasamy, B. Baranowski, The "uphill" diffusion of hydrogen-strain- gradient-induced effects in palladium alloy membranes, Platin. Met. Rev. 32 (1988) 22–26.

[10] P. Tripodi, N. Armanet, V. Asarisi, A. Avveduto, A. Marmigi, J.-P. Biberian, J.D. Vinko, The effect of hydrogen stoichiometry on palladium strain and resistivity, Phys. Lett. A 373 (2009) 4301–4306.

[11] W. Luo, D.F. Cowgill, K. Stewart, Absorption isotherms for H$_2$(D$_2$)-Pd$_{0.8}$Ag$_{0.2}$ (198-323 K), J. Alloys Compd. 489 (2010) 47–50.

[12] M.L.H. Wise, J.P.G. Farr, I.R. Harris, X-ray studies of the α/β miscibility gaps of some palladium solid solution-hydrogen systems, J. Less Common. Met. 41

[13] (1975) 115–127.

[13] A. Pozio, Z. Jovanovic, R. Lo Presti, M. De Francesco, S. Tosti, Pd-Ag hydrogen content and electrical resistivity: temperature and pressure effect, Int. J. Hydrogen Energy 37 (2012) 7925–7933.

[14] M. Catti, O. Fabelo, A. Filabozzi, A. Pietropaolo, S. Tosti, A. Pozio, A. Santucci, Neutron diffraction study of the Pd$_{0.772}$Ag$_{0.228}$D$_v$ membrane for hydrogen separation, Int. J. Hydrogen Energy 42 (2017) 6787–6792.

[15] J. Rodriguez-Carvajal, Recent advances in magnetic structure determination by neutron powder diffraction, Physica B 192 (1993) 55–69. The programs of the FullProf Suite can be obtained at, http://www.ill.eu/sites/fullprof.

[16] P. Thompson, D.E. Cox, J.B. Hastings, Rietveld refinement of Debye-Scherrer synchrotron X-ray data from Al$_2$O$_3$, J. Appl. Crystallogr. 20 (1987) 79–83.

[17] M.P. Pitt, E.M. Gray, Tetrahedral occupancy in the Pd-D system observed by *in situ* neutron powder diffraction, Europhys. Lett. 64 (2003) 344–350.

[18] K.G. Mc Lennan, E.M. Gray, J.F. Dobson, Deuterium occupation of tetrahedral sites in palladium, Phys. Rev. B 78 (2008), 014104 1-9.

[19] R. Lasser, Isotope dependence of phase boundaries in the PdH, PdD, and PdT systems, J. Phys. Chem. Solids 46 (1985) 33–37.

[20] T. Mohri, W.A. Oates, CVM-based calculation of the Pd-H phase diagram in the high temperature region, Mater. Trans. 43 (2002) 2656–2661.

[21] J.-M. Joubert, S. Thiébaut, Thermodynamic assessment of the Pd-H-D-T system, J. Nucl. Mater. 395 (2009) 79–88.

[22] S. Dekura, H. Kobayashi, R. Ikeda, M. Maesato, H. Yoshino, M. Ohba, T. Ishimoto, S. Kawaguchi, Y. Kubota, S. Yoshioka, S. Matsumura, T. Sugiyama, H. Kitagawa, The electronic state of hydrogen in the α phase of the hydrogen-storage material PdH[D]$_x$: does a chemical bond between palladium and hydrogen exist ? Angew. Chem. Int. Ed. 57 (2018) 9823–9827.

[23] T.B. Flanagan, D. Wang, S. Luo, Thermodynamics of H in disordered Pd-Ag alloys from calorimetric and equilibrium pressure-composition-temperature measurements, J. Phys. Chem. B 111 (2007) 10723–10735.

[24] N.S. Anand, S. Pati, R.A. Jat, S.C. Parida, S.K. Mukerjee, Thermodynamics and kinetics of hydrogen/deuterium absorption-desorption in Pd$_{0.77}$Ag$_{0.23}$ alloy, Int. J. Hydrogen Energy 40 (2015) 444–450.

[25] T.B. Flanagan, S. Luo, Thermodynamics of hydrogen solution and hydride formation in binary Pd alloys, J. Phase Equilib. Diffus. 28 (2007) 49–57.

[26] A. Khawam, D.R. Flanagan, Solid-state kinetic models: basics and mathematical fundamentals, J. Phys. Chem. B 110 (2006) 17315–17328.

[27] Y. Pang, Q. Li, A review on kinetic models and corresponding analysis methods for hydrogen storage materials, Int. J. Hydrogen Energy 41 (2016) 18072–18087.

[28] Y. Sakamoto, S. Hirata, H. Nishikawa, Diffusivity and solubility of hydrogen in Pd-Ag and Pd-Au alloys, J. Less Common. Met. 88 (1982) 387–395.

[29] Y. Jin, L. Wang, M. Hara, K. Watanabe, Kinetics of hydrogen isotope absorption for well-annealed palladium-platinum alloys, Mater. Trans. 48 (2007) 560–565.

[30] D. Wang, T.B. Flanagan, K. Shanahan, Diffusion of H through Pd-Ag alloys, J. Phys. Chem. B 112 (2008) 1135–1148.